Valorization of Municipal Biowaste into Electrospun Poly(3-hydroxybutyrate- co-3-hydroxyvalerate) Biopapers for Food Packaging Applications

MELENDEZ-RODRIGUEZ, B., TORRES-GINER, S., LORINI, L., VALENTINO, F., SAMMON, Chris <http://orcid.org/0000-0003-1714-1726>, CABEDO, L. and LAGARON, J.M.

Valorization of Municipal Biowaste into Electrospun Poly(3-hydroxybutyrate-*co*-3-hydroxyvalerate) Biopapers for Food Packaging Applications

Beatriz Melendez-Rodriguez[1], Sergio Torres-Giner[1], Laura Lorini[2], Francesco Valentino[2], Chris Sammon[3], Luis Cabedo[4], and Jose Maria Lagaron[1*]*

[1] Novel Materials and Nanotechnology Group, Institute of Agrochemistry and Food Technology (IATA), Spanish Council for Scientific Research (CSIC), Paterna, Spain.

E-mails: lagaron@iata.csic.es, storresginer@iata.csic.es

[2] Department of Chemistry, "La Sapienza" University of Rome, Rome, Italy

[3] Materials and Engineering Research Institute, Sheffield Hallam University, Sheffield, United Kingdom

[4] Polymers and Advanced Materials Group (PIMA), Universitat Jaume I (UJI), Castellón, Spain

Abstract. In the present study, highly sustainable poly(3-hydroxybutyrate-*co*-3-hydroxyvalerate) (PHBV) was produced by mixed bacterial cultures derived from municipal biowaste (MBW). After purification and extraction, the MBW derived PHBV was processed by electrospinning to yield defect-free ultrathin fibers, which were thermally post-treated. Annealing at 130°C, well below the polymer melting point, successfully yielded a continuous film resulting from coalescence of the fibrilar morphology, so-called biopaper, exhibiting enhanced optical and colour properties compared to traditional melt compounding routes. The crystallinity and crystalline morphology were comprehensively studied as a function of temperature by ATR-FTIR spectroscopy and combined time resolved synchrotron SAXS and WAXS experiments, which revealed that the molecular order within the copolyester was improved up to a maximum at 130^{o}C, and then decreased at the polymer melting point. It is hypothesized that by annealing at the temperature at which thermally induced molecular order is maximized, the fibers generate sufficient mobility to align side by side hence reducing surface energy and porosity. The data suggest that this material has a good balance between enhanced mechanical and improved barrier properties to vapours and gases in comparison to other currently used petroleum based polymers, hence presenting significant potential to be part of innovative food biopackaging designs for the protection and preservation of foods in the frame of the Circular Bioeconomy concept.

Keywords: PHBV, electrospinning, biopapers, waste valorization, food packaging, Circular Bioeconomy

1. Introduction

The potential of polyhydroxyalkanoates (PHAs) as bio-based and biodegradable replacements for conventional bulk commodity plastic packaging while promoting sustainable development has long been recognized [1]. These biopolymers are produced by the action of bacteria, both Gram-positive (G+) and Gram-negative (G-) [2], during the fermentation of sugar or lipids in famine conditions [3]. The most studied is poly(3-hydroxybutyrate) (PHB or P3HB), which possesses similar thermal and mechanical properties to some synthetic polymers such as polypropylene (PP) and low-density polyethylene (LDPE) [4-5]. However, the homopolyester shows low ductility and toughness and a narrow processing window, which limits its use for packaging applications. For this reason, its copolymer with 3-hydroxyvalerate (HV), *i.e.*, poly(3-hydroxybutyrate-*co*-3-hydroxyvalerate) (PHBV), with associated lower crystallinity, decreased stiffness, and also lower melting temperature (T_m), is a more interesting candidate in the areas of biodegradable packaging [6].

Current manufacturing processes of PHAs by bacterial fermentation involve fermentation, isolation, and purification from the fermentation broth [7-8]. Much effort and improvements are currently being taken to reduce the costs of the fermentation and downstream processes [9], which can be up to 15 times higher than conventional polyolefins [10]. The production of PHAs by mixed microbial cultures (MMCs) using biowaste as feedstock, such as industrial waste and food processing by-products, can make its industrial production more competitive [11]. In fact, pure culture systems based on refined feedstock and sterile cultivation conditions contribute most to the PHA production cost [12]. Furthermore, the use of by-products and waste is environmentally attractive in a Circular Bioeconomy context [13]. In this regard, different organic wastes

have been used as substrates to produce PHAs, such as molasses [14], olive and palm oil mill effluent [15-16], fermented fruit waste [17-18], and cheese whey [19].

The municipal waste, wastewaters and the organic fraction of the municipal solid waste (OFMSW), also show a great potential as the feeding solution for the PHA production. However, to date, few studies have reported the use of the OFMSW in the production of these biopolymers [20]. Along with the production of biogas, composting or anaerobic digestion are two of the most common processes applied to biological sludge disposal in order to stabilize organic matter and valorize different substrates into added-value marketable products [21]. Other studies have reported the use of OFMSW during the accumulation step to enrich to a PHA producing community on a volatile fatty acid (VFA) solution improved the PHA productivity [22]. Another study demonstrated that the PHA accumulation fed with fermentation VFAs, from food wastes and excess sludge, was higher than that with analytically pure VFAs [23]. PHA production has also been reported utilising an MMC indigenous to an activated sludge process on carbon present in municipal wastewaters[24]. Therefore, the integration of the so-called MMC−PHA production in these kinds of infrastructures by using activated sludge as an inoculum can make this technology economically and environmentally sustainable.

Electrospinning is a innovative technique that allows the formation of continuous polymer fibers, with range diameters between several nanometers to a few microns, through the application of an external high-voltage electric field [25]. The size and morphology of the resultant fibrous mat depends on the polymer solution properties, that is, viscosity, surface tension, and conductivity, and also the process conditions, that is, applied voltage, flow-rate, and tip-to-collector distance [26]. A thermal post-treatment below the polymer's melting point (T_m) of the electrospun polymer mats yields the formation of fiber-based continuous films, also called biopapers, due to the coalescence

and rearrangement of the nanofibers. This makes the use of electrospun films of PHA a very interesting alternative in the packaging industry since continuous films can be obtained with minimal thermal exposure that can exhibit improved optical, mechanical strength and flexibility with excellent barrier properties [27-28]. Moreover, this technique allows the formation of coatings or interlayers of interest in packaging by the incorporation into the biopolymers of nanofillers and active substances [29-35].

The objective of this study was to valorize, for the first time, typical municipal biowaste streams into so-called biopapers of PHBV produced by annealing of electrospun fibers, and then asses the resulting morphology, crystallinity and crystalline morphology as a function of temperature, and physico-chemical properties relevant for food biopackaging applications.

2. Experimental

2.1. Materials

The PHBV copolyester was produced at the pilot platform in the Treviso Municipal Wastewater Treatment Plant (Treviso, Italy). The biopolymer was produced from a feedstock composed from a mixture of the liquid slurry resulting from squeezing of the organic fraction of municipal solid waste (OFMSW) and the biological sludge from the treatment of urban wastewater. A commercial PHBV grade, ENMAT^{TM} Y1000P produced by Tianan Biologic Materials (Ningbo, China) and supplied by Ocenic Resins S.L., Spain, was also used for comparison. According to the manufacturer, the 3HV fraction in the copolyester is 2–3 mol%.

2,2,2-trifluoroethanol (TFE), ≥99% purity, $_D$-limonene, with 98% purity, 1-butanol, reagent grade with 99.5% purity, methanol, sulfuric acid, and benzoic acid were all

purchased from Sigma-Aldrich S.A. (Madrid, Spain). Chloroform, stabilized with ethanol and 99.8% purity, was obtained from Panreac S.A. (Barcelona, Spain).

2.2. Production of unpurified PHBV powder

The PHBV production consisted of three process steps using the fermented mixture of the organic fraction of municipal solid waste (OFMSW) and the biological sludge. In the first stage, the precursors for PHA biosynthesis, that is, the volatile fatty acids (VFAs), were produced in an anaerobic fermentation reactor of 380 L. Then, biomass cultivation was carried out in a second aerobic reactor, referred to as the sequencing batch reactor (SBR) of 100 L. Finally, a third fed-batch aerobic reactor of 70–90 L was used for PHA accumulation within the cellular wall. At the end of the accumulation step, the PHA concentration reached up to a value of 2.0–2.5 g/L, corresponding to a maximum PHA content of 50–60% of cell dry weight, that is, mass ratio of PHA vs. volatile solids. This PHA-rich, raw biomass, was collected following a protocol addressed to the long-term PHA conservation inside the cells before the extraction/purification steps. In this protocol, at the end of each accumulation, the PHA-rich biomass was left to settle under gravity and, thereafter, the thickened slurry was centrifuged for 15 min at 4500 rpm in a Heraeus™ Megafuge™ 40 Centrifuge from Thermo Fisher Scientific (Waltham, MA, USA). The wet pellet was thermally pretreated at 145°C for 15 min and then dried overnight at 60°C. A more detailed description of the production process was described by Valentino et al. [36].

2.3. Extraction and purification of PHBV powder

The unpurified PHBV was extracted using the chloroform-based extraction method reported previously [37]. For this, the MBW derived PHBV was dissolved in chloroform

at 5 wt.% and the mixture was stirred for 24 h at 50 ºC to degrade the non-PHA cellular material. Next, the solution was transferred to centrifugation tubes in which distilled water was added at 50 wt.%. After shaking the tubes manually, these were centrifuged for 5 min at 4000 rpm in an Avanti J-26S XP Centrifuge from Beckman Coulter, Inc. (Brea, CA, USA). Finally, the PHBV suspension was recovered from the bottom of the tubes with a pipette and transferred to beakers, leaving them in the extractor hood until the solvent was completely evaporated.

2.4. 3HV content determination in the dry samples

A powder sample of 3.5 mg was suspended in 2 mL of acidified methanol solution (3% vol/vol H_2SO_4), containing benzoic acid at 0.005 % w/v as internal standard, and 1 mL of chloroform in a screw-capped tube. An acid-catalyzed methanolysis occurred and the 3-hydroxyacyl methyl esters of PHA were quantified by gas–chromatography in a GC-FID Perkin Elmer 8410 from PerkinElmer, Inc. (Waltham, MA, USA). The relative abundance of 3HB and 3HV monomers was determined using as a reference standard of commercial PHBV copolymer with a known 3HV content of 5 wt% (Sigma–Aldrich S.r.l., Milan, Italy). The resultant molar fraction of 3HV in the copolyester was approximately 10 wt%.

2.5. Characterization of the PHBV solutions

The powder resulting from the purification process was dissolved in a mixture of chloroform and butanol 75:25 (wt./wt.) at 15 wt.% under magnetic stirring for 24 h at 50 ºC. The PHBV solution was characterized in terms of its viscosity, conductivity, and surface tension prior to electrospinning. A solution of commercial PHBV was also prepared by dissolving the biopolymer at 10 wt.% in TFE for comparison. The apparent

viscosity (ηa) was determined at 100 s^{-1} using a rotational viscometer Visco BasicPlus L from Fungilab S.A. (San Feliu de Llobregat, Spain) equipped with a low-viscosity adapter (LCP). The conductivity was evaluated using a conductivity meter XS Con6 from Lab-box (Barcelona, Spain). The surface tension was measured via the Wilhemy plate method using an EasyDyne K20 tensiometer from Krüss GmbH (Hamburg, Germany). All measurements were conducted at room temperature in triplicate.

2.6. Electrospinning process

The PHBV solutions were thereafter processed by electrospinning using a Fluidnatek® LE-10 lab equipment manufactured by Bioinicia S.L. (Valencia, Spain). The equipment has a motorized single needle injector, scanning horizontally towards a metallic fixed collector. The conditions for processing the MBW PHBV were optimal at a flow-rate of 6 mL/h, 22 kV of voltage, and 25 cm of needle-to-collector distance. In the case of the commercial PHBV, electrospinning was carried out using previously optimized conditions, that is, flow-rate of 6 mL/h, 20 kV of voltage, and a needle-to-collector distance of 15 cm [38]. The PHBV solutions were electrospun for 1.3 h at 25 ºC and 40% relative humidity (RH). All the manufactured mats were stored in the darkn at room temperature in a desiccator at 0% RH for at least a week before thermal post-treatment.

2.7. Preparation of the PHBV biopapers from electrospun fibers

The resultant electrospun mat of PHBV derived from MBW was subjected to the annealing process in a 4122-model press from Carver, Inc. (Wabash, IN, USA). This process was performed across the temperature range 80 ºC to 150 ºC, for 5 seconds and without pressure. The electrospun mat of commercial PHBV was annealed at 155 °C,

for 5 s, without pressure [38]. All the thermally post-processed samples had an average thickness of approximately 30 μm. The samples were stored in a desiccator at 0% RH for two weeks before characterization.

2.8. Characterization of the PHBV biopapers

2.8.1. Scanning electron microscopy

The morphology of the electrospun PHBV fibers and resultant biopapers were determined using scanning electron microscopy (SEM) using an S-4800 instrument from Hitachi (Tokyo, Japan). For the cross-section observations, the films were cryo-fractured by immersion in liquid nitrogen. Prior to observation, the samples were fixed to beveled holders using conductive double-sided adhesive tape and sputtered with a mixture of gold-palladium under vacuum. An accelerating voltage of 10 kV was used and the estimation of the dimensions was performed by means of the Aperture software from Apple (Cupertino, CA, USA) using a minimum of 20 SEM micrographs in their original magnification.

2.8.2. Transparency

The light transmission of the biopapers was determined using specimens of 50 mm × 30 mm by quantifying the absorption of light at wavelengths between 200 nm and 700 nm in an ultraviolet–visible (UV–vis) spectrophotometer VIS3000 from Dinko Instruments (Barcelona, Spain). The transparency (T) and opacity (O) were calculated using Equations 1 [39] and 2 [40], respectively:

$$T = \frac{A600}{L} \quad (1)$$

$$O = A_{500} \cdot L \quad (2)$$

where A500 and A600 are the absorbance values at 500 nm and 600 nm, respectively, and L is the film thickness (mm).

2.8.3. Color measurements

The biopapers color was determined using a chroma meter CR-400 (Konica Minolta, Tokyo, Japan). The color difference (ΔE*) was determined, as defined by the Commission Internationale de l'Eclairage (CIE), using Equation 3 [41]:

$$\Delta E^* = [(\Delta L^*)^2 + (\Delta a^*)^2 + (\Delta b^*)^2]^{0.5} \quad (3)$$

where ΔL*, Δa*, and Δb* correspond to the differences in terms of lightness from black to white, color from green to red, and color from blue to yellow, respectively, between the test sample and the control sample of commercial PHBV. Color change was evaluated using the following assessment: Unnoticeable ($\Delta E^* < 1$), only an experienced observer can notice the difference ($\Delta E^* \geq 1$ and < 2), an unexperienced observer notices the difference ($\Delta E^* \geq 2$ and < 3.5), clear noticeable difference ($\Delta E^* \geq 3.5$ and < 5), and the observer notices different colors ($\Delta E^* \geq 5$) [42].

2.8.4. Thermal analysis

Thermal transitions were studied using differential scanning calorimetry (DSC) on a DSC-7 analyzer from PerkinElmer, Inc. (Waltham, MA, USA), equipped with a cooling accessory Intracooler 2 also from PerkinElmer, Inc. A three-step program, under nitrogen atmosphere with a flow-rate of 20 mL/min, was applied: a first heating step from -30 to 180 ºC, followed by a cooling step back to -30 ºC, and completed by a second heating to 200 ºC. The heating and cooling rates were set to 10 ºC/min and the

typical sample weight was ~3 mg, while an empty aluminum pan was used as reference. Calibration was performed using an indium sample and the thermograms were corrected with those of an empty pan. All tests were carried out in triplicate. The melting temperature (T_m) and enthalpy of melting (ΔH_m) were obtained from the first heating scan, while the crystallization temperature from the melt (T_c) and enthalpy of crystallization (ΔH_c) were determined from the cooling scan.

Thermogravimetric analysis (TGA) was performed in a TG-STDA model TGA/STDA851e/LF/1600 thermobalance from Mettler-Toledo, LLC (Columbus, OH, USA). The samples, with a weight of about 15 mg, were heated from 50 ºC to 900 ºC, at a heating rate of 10ºC/min under a nitrogen flow-rate of 50 mL/min.

2.8.5. Attenuated Total Reflectance-Fourier Transform Infrared (ATR-FTIR) spectroscopy

Variable temperature FTIR was performed on a Nicolet Nexus FTIR instrument (Thermo Fisher Scientific, Wilmington, DE, USA) coupled to a variable temperature single reflection diamond ATR sampling accessory (Specac Ltd., Orpington, UK). Spectra were collected by averaging 64 scans at 4 cm^{-1} resolution using the blank ATR crystal at the same temperature as the background. The intensity of an infrared spectrum depends on a number of factors including path length and the molar extinction coefficient of the analyte. When using the ATR geometry the path length can be considered to be constant as long as the contact between the sample and the ATR crystal is consistent. To ensure that any peak intensity changes in the data represented changes to the morphology of the samples, the samples were clamped directly onto the ATR crystal using a calibrated torque wrench (Specac Ltd., Orpington, UK) set at 80 cNm, which applies a load of ~350N via the sample accessory anvil. Reproducibility of the

sample contact and resulting spectra intensity were validated prior to conducting the variable temperature infrared measurements. Spectra were collected at 10 ºC intervals from 30 ºC to 100 ºC and, thereafter, at 5 ºC intervals up to 190 ºC. To ensure the validity of the selected temperature, spectra were not collected until the digital reading on the temperature controller had fully stabilised.

2.8.6. Time-resolved synchrotron X-ray scattering

Simultaneous Small Angle X-Ray Scattering (SAXS) and Wide Angle X-Ray Scaterring (WAXS) experiments as a function of temperature were carried out on beam line BL11 – Non-crystalline diffraction (NCD) (WAXS/SAXS station) located at the ALBA synchrotron facilities (Barcelona, Spain). The SAXS and WAXS q-axis calibration were obtained by measuring silver behenate ($AgC_{22}H_{43}O_2$) and chromium (III) oxide (Cr_2O_3) standards, respectively. Scattering patterns were collected using the combination of two detectors, that is, a photon counting detector Pilatus 1M detector from Dectris AG (Baden, Switzerland) and a CDD WAXS LX255-HS detector from Rayonix, L.L.C. (Evanston, IL, USA), operating simultaneously in SAXS and WAXS positions, respectively. The wavelength of the incident wave (λ) was 1 Å. Distances between the sample and SAXS and WAXS detectors were fixed at 6.6328 m and 0.120762 m, respectively, allowing a q range between 0.025 – 0.22 $Å^{-1}$ for SAXS and a q-range between 0.5 – 8.4 $Å^{-1}$ for WAXS. The beamline delivered a photon flux onto the sample of > 1.5 x 10^{12} ph/s at 12.4 KeV for a beam current of 150 mA with a bandpass ($\Delta E/E$) of 2.7 x 10^{-4} at 10.0 keV and a beam size at sample position of 349 µm x 379 µm. For the *in situ* thermal experiments, electrospun mats, with a thickness of 100 µm, were placed on a hot stage "film type" THMS600 from Linkam Scientific Instruments Ltd (Epstom, UK). To analyze the evolution of the sample when exposed to

thermal treatments, the samples were subjected to isotherms at 100 °C and 130 °C for up to 2 min and to thermal ramps from 0 °C to 180 °C at 10 °C/min.

2.8.7. Tensile tests

Tensile tests of the PHBV biopapers were performed according to ASTM standard method D638 using an Instron 4400 universal testing machine from Instron (Norwood, MA, USA). The tests were performed, under ambient conditions, with 115 mm × 16 mm stamped dumb-bell shaped specimens using a cross-head speed of 10 mm/min. This was equipped with a 1-kN load cell. Samples were conditioned to the test conditions for 24 h prior to tensile assay. At least six specimens were measured for each biopaper and the average results with standard derivation were reported.

2.8.8. Permeability tests

The water vapor permeability (WVP) of the PHBV biopapers was determined using the gravimetric method ASTM E96-95 performed in triplicate. For this, 5 mL of distilled water was placed inside a Payne permeability cup (diameter of 3.5 cm) from Elcometer Sprl (Hermallesous-Argenteau, Belgium). The sample was not in direct contact with water but exposed to 100% RH on one side and secured with silicone rings. The cups were placed within a desiccator containing silica gel at 0% RH in a cabinet at 25 ºC. Control samples using cups with aluminum films to estimate solvent loss through the sealing were subjected to the same experimental conditions. The cups were weighted periodically using an analytical balance (±0.0001 g). WVP was calculated from the regression analysis of weight loss data versus time, and the weight loss was calculated as the total loss minus the loss through the sealing. The permeability was obtained by multiplying the permeance by the film thickness.

Limonene permeability (LP) was measured using the approach described above for WVP, by placing 5 mL of $_{D}$-limonene inside the Payne permeability cup. The cups containing the samples were placed at the controlled room conditions of 25 ºC and 40% RH. The samples were measured in triplicate and limonene vapor permeation rates were estimated from the steady-state permeation slopes and weight loss was calculated as the total cell loss minus the loss through the seal. The LP values were calculated taking into account the average film thickness in each case.

The oxygen permeability coefficient was derived from the oxygen transmission rate (OTR) measurements that were recorded at 60% RH and 25 ºC, in duplicate, using an Oxygen Permeation Analyzer M8001 (Systech Illinois, Thame, UK). The samples were previously purged with nitrogen in the humidity equilibrated samples, before exposure to an oxygen flow of 10 mL/min. The exposure area during the test was 5 cm^2 for each sample. In order to obtain the oxygen permeability (OP), film thickness and gas partial pressure were considered.

2.8.9. Statistical Analysis

The solution properties and the optical, thermal, mechanical, and barrier properties of the biopapers were evaluated through analysis of variance (ANOVA) using STATGRAPHICS Centurion XVI v 16.1.03 from StatPoint Technologies, Inc. (Warrenton, VA, USA). Fisher's least significant difference (LSD) was used at the 95% confidence level ($p < 0.05$). Mean values and standard deviations were also reported.

3. Results and discussion

3.1. Morphology of the electrospun PHBV mats and biopapers

The values of viscosity, surface tension, and conductivity of the MBW derived PHBV solution were measured and reported in **Table 1** in order to evaluate its electrospinnability. One can observe that the MBW derived PHBV solution presented a viscosity of 229.8 cP, which was significantly lower than that attained for the PHBV commercial benchmark, (~689 cP), even though the concentration of the commercial biopolymer in the solution being lower. This can be related to the different solvents used for the solution, as well as the higher HV content and potentially lower molecular weight (M_W) of the MBW derived PHBV. In this regard, not only can the feedstock used to feed the microorganisms affect the M_W of the resultant PHA but also the chemical digestion methods adopted to disrupt the cell wall and release PHAs [43]. In any case, the attained value of viscosity is appropriate for electrospinning since it was similar to that reported for solutions containing 2 wt.% of PHBV obtained from fruit pulp biowaste purified using chloroform, that is, 296.8 cP [17]. In the case of surface tension and conductivity, the MBW derived PHBV solution presented a value of 26.2 mN/m and 0.14 µS/cm, respectively. The surface tension was very similar for both PHBV solutions and also comparable to other PHAs derived from biowaste, which were reported in the 20.5–21.9 mN/m range, but the conductivity was lower, that is, 1.3–3.7 µS/cm range [17]. This is a positive indicator for electrospinning since polymer solutions with high conductivities usually show lower processability [44].

Table 1. Properties of the poly(3-hydroxybutyrate-*co*-3-hydroxyvalerate) (PHBV) derived from municipal biowaste (MBW) and commercial grade solutions.

Sample	**Concentration (wt%)**	**Viscosity (cP)**	**Surface tension (mN/m)**	**Conductivity (µS/cm)**

Commercial PHBV	10	688.8 ± 2.3[a]	21.9 ± 0.1[a]	3.74 ± 0.02[a]
MBW derived PHBV	15	229.8 ± 1.5[b]	26.2 ± 0.3[b]	0.14 ± 0.01[b]

[a–b] Different letters in the same column indicate a significant difference among the samples ($p < 0.05$).

Figure 1 shows the resultant electrospun mats obtained from the MBW derived PHBV solutions, before and after annealing, both the cryo-fracture surfaces and the top views. One can observe in the figure at room temperature, which corresponds to the electrospun mat without thermal post-treatment, that the electrospinning process generated a mat composed of non-woven ultrathin fibers. In particular, the electrospinning of the PHBV solution yielded bead-free and homogenous fibers with a mean diameter of 1.12 ± 0.12 μm. It can also be observed that the application of annealing temperatures of 80 ºC, 110 ºC, and 125 ºC resulted in a rearrangement of the fine fibers but the material still maintained a high porosity level. At 130 ºC, interestingly, the electrospun PHBV mat turned into a continuous film with a very low porosity due to a fiber coalescence process. This phenomenon has been ascribed to the compact packing rearrangement to reduce surface energy of the electrospun fibers at temperatures below the biopolymer's T_m [45]. **Figure 2** displays, as an example, a zoomed top view of the biopaper annealed at 130 ºC, that proved that the material is constituted by aligned side by side fibers of ca. 1.2 to 2 microns with minimal porosity. The resultant morphology has been recently termed as "biopaper" since it refers to fiber-based continuous films made of natural polymers that are non-fiber based in origin, as is the case of PHAs, in resemblance to the concept of conventional papers made of cellulosic fibers [46].

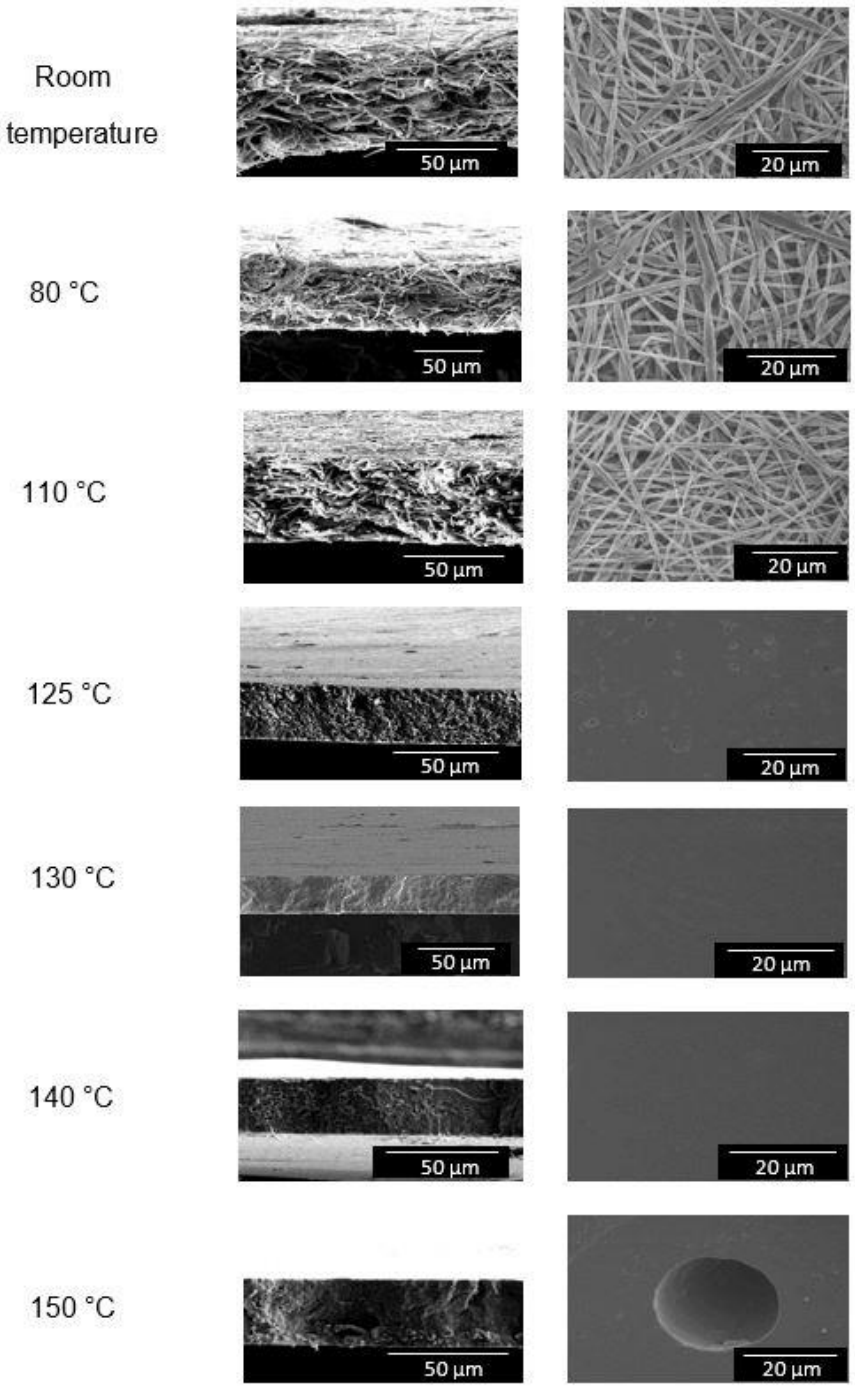
Room temperature
50 µm
20 µm
80 °C
50 µm
20 µm
110 °C
50 µm
20 µm
125 °C
50 µm
20 µm
130 °C
50 µm
20 µm
140 °C
50 µm
20 µm
150 °C
50 µm
20 µm

Figure 1. Scanning electron microscopy (SEM) images of the cross-section (left) and top view (right) of the electrospun municipal biowaste (MBW) derived poly(3-hydroxybutyrate-*co*-3-valerate) (PHBV) mats without thermal post-treatment and annealed at 80 ºC, 110 ºC, 125 ºC, 130 ºC, 140 ºC, and 150 ºC for 5 seconds. Scale markers are of 50 µm and 20 µm, respectively.

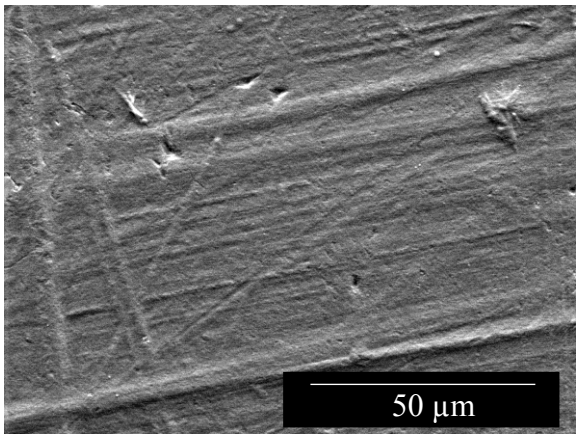

Figure 2. Scanning electron microscopy (SEM) image of the top views of the electrospun MBW derived PHBV mats annealed at 130 ºC. Scale marker is of 50 µm.

Figure 1 also shows that at higher temperatures, i.e. at 150 ºC, some large voided areas were formed, which could be the result of thermal deterioration and release of volatile components. A similar film morphology evolution was recently observed for electrospun fibers mats of a fruit residues derived PHBV [17]. Based on the morphology observations, the electrospun mats post-processed at 130 ºC were selected for further characterization.

3.2. Optical Properties of the PHBV biopapers

Figure 3 displays the background transparency pictures of resulting annealed electrospun mats of MBW derived and commercial PHBV. It can be observed that both biopapers show certain transparency and lack of color, suggesting that the PHBVs presented low crystallinity and were not thermally abused, respectively. Electrospinning is known to result in low crystallinity materials due to the very rapid solidification process of the polymer jet. In the case of the MBW derived PHBV, the samples show even higher transparency associated to the higher HV content which is known to yield lower melting point, crystallinity and density materials.

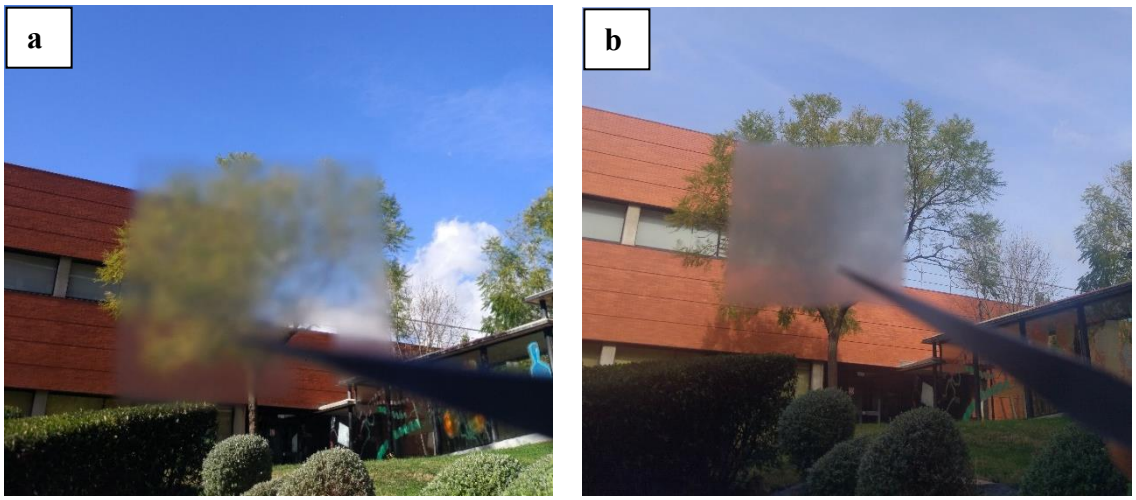

Figure 3. Background transparency pictures of the electrospun poly(3-hydroxybutyrate-*co*-3-valerate) (PHBV) biopapers of: (a) derived from municipal biowaste (MBW) and (b) commercial grade.

To quantify the color properties of the electrospun PHBV biopaper, the lightness and color parameters were determined by the values of L* and a* b* coordinates, respectively. One can observe in **Table 2** that the MBW derived PHBV biopaper showed a value of L* of 89.39 while the values of a* and b* were -0.2 and 2.13, indicating that it was relatively luminous and only slightly yellow. These values were very similar to those obtained for the electrospun films of PHBV derived from wastes of

fruit pulp, thought the present samples showed slightly higher values of a* and b* [47]. Interestingly, the electrospun biopapers were brighter than PHB/PHBV blend films obtained by melt processing routes, which showed a value of L* of 86.40 [48]. In terms of color difference, the electrospun biopaper made of MBW derived PHBV showed a color difference of 1.03, which is nearly unnoticeable ($\Delta E^* < 1$) and it can be noticed only by an experienced observer ($\Delta E^* \geq 1$ and < 2). Regarding transparency and opacity, one can also observe that the MBW derived PHBV biopaper presented a higher value of T and lower value of O than the biopaper made from commercial PHBV, which means that biopaper obtained from MBW was more transparent and developed a less grayish color than the commercial one. This optical property can be regarded as an advantage for food packaging because transparency is associated with conventional plastics used in packaging and is better accepted by users. In this regard, Jung et al. [49] induced a color change from yellowish to bluish in PHB films to make them more commercially attractive.

Table 2. Optical properties of the electrospun poly(3-hydroxybutyrate-*co*-3-hydroxyvalerate) (PHBV) derived from municipal biowaste (MBW) and commercial grade biopapers.

Film	a*	b*	L*	ΔE*	T	O
Commercial PHBV	0.35 ± 0.03^{a}	1.29 ± 0.01^{a}	89.14 ± 0.02^{a}	-	9.20 ± 0.08^{a}	0.07 ± 0.02^{a}
MBW derived PHBV	-0.20 ± 0.02^{b}	2.13 ± 0.03^{b}	89.39 ± 0.03^{a}	1.03 ± 0.02	2.56 ± 0.02^{b}	0.01 ± 0.001^{b}

*a**: red/green coordinates (+a red, −a green); *b**: yellow/blue coordinates (+b yellow, −b blue); *L**: Luminosity (+L luminous, −L dark); *ΔE**: color differences; T: transparency; O: opacity. $^{a-c}$ Different letters in the same column indicate a significant difference among the samples *($p < 0.05$)*.

3.3. Thermal properties

Additional characterization was only performed on the MBW material since the full physico-chemical characterization of the commercial material has been published previously [38].

The DSC curves, for the first heating and cooling steps, of the MBW PHBV biopaper are collated in **Figure 4**. **Table 3** summarises the main thermal values obtained from DSC. During the first heating, the sample showed a multiple melting endotherm with ΔH_m at ca. 58 J/g. In the cooling step, it can be observed that the film crystallized from the melt in a single step, showing a clear crystallization peak (T_c) at 68 ºC. The presence of multiple melting peaks in a relatively low thermal range is linked to a dynamic crystal reorganization upon heating by which imperfect crystals order into spherulites with thicker lamellar thicknesses, which then melt at higher temperatures. This phenomenon was previously observed and discussed by, among others, Zhang et al. [50] in PHA copolyesters. In comparison with other PHBV films with different HV contents, Sanchez-Garcia et al. [51] showed that copolyesters with HV 12 mol% exhibited double melting with peaks centered at approximately 145 ºC and 157 ºC. Elsewhere, Castro-Mayorga et al. [52] showed that PHBV blends with HVs of 3 mol% and 18 mol% also presented double melting peaks with T_m values of 169.6 ºC and 173.2 ºC. In the case of the homopolyester, PHB only showed one melting peak at 169.4 ºC [45]. Due to their higher HV contents, the T_m values of MBW derived PHBV were lower than PHB ones and slightly higher than those obtained for PHBV derived from fruit pulp waste with 20 mol% of HV content, with a single melting peak at 139 ºC [17].

In **Table 3** the thermal stability values of the MBW derived PHBV biopapers obtained from TGA are also included. It can be observed that the copolyester presented an onset-degradation temperature (T_{onset}), defined as the temperature at 5% weight loss, of ~205 ºC. Its thermal degradation temperature (T_{deg}) occurred at ~240 ºC, associating

a mass loss of approximately 95% whereas the amount of residual mass was 0.2%. These results are in agreement with previous films of PHBV with a HV content of 18 mol%, which were thermally stable up to 249.8 ºC [53]. However, other studies reported that PHBV with different HV contents showed higher thermal stability. For instance, PHBV with 20% HV showed $T_{5\%}$ and T_{deg} values of approximately 267 °C and 290 °C, respectively [17], while commercial PHBV with a HV content of 3 mol% showed a $T_{5\%}$ value of 269 °C and a T_{deg} value of 290.8 °C [54]. This observation points out that thermal stability was not only dependent on the HV content but it was also related to other factors such M_W, purity or the presence of additives.

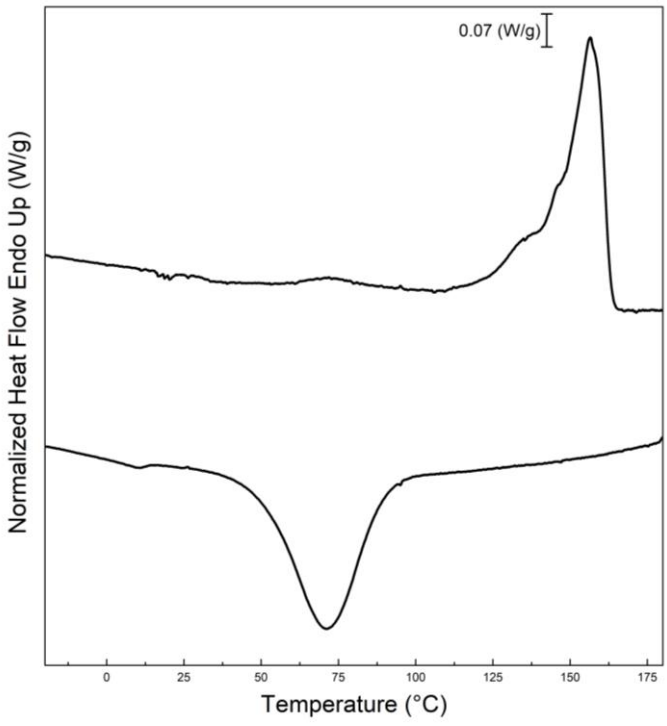

Figure 4. Differential scanning calorimetry (DSC) curves during first heating and cooling of the electrospun biopapers of poly(3-hydroxybutyrate-*co*-3-valerate) (PHBV) derived from municipal biowaste (MBW).

Table 3. Thermal properties of the electrospun municipal biowaste (MBW) derived poly(3-hydroxybutyrate-*co*-3-hydroxyvalerate) (PHBV) fibers obtained from differential scanning calorimetry (DSC) and thermogravimetric analysis (TGA) in terms of: Main melting temperature (T_m), enthalpy of melting (ΔH_m), crystallization temperature (T_c), enthalpy of crystallization (ΔH_c), onset degradation temperature (T_{onset}), degradation temperature (T_{deg}), and residual mass at 800 ºC.

	DSC			
	T_m (ºC)	**ΔH_m (J/g)**	**T_c (ºC)**	**ΔH_c (J/g)**
PHBV	155.4 ± 1.5	57.6 ± 2.2	68.1 ± 4.1	43.9 ± 8.2
	TGA			
	$T_{5\%}$ (ºC)	**T_{deg} (ºC)**	**Mass loss (%)**	**Residual mass (%)**
	204.7 ± 2.0	239.9 ± 0.8	94.8 ± 1.7	0.2 ± 0.1

3.4. Crystalline Morphology

Figure 5 shows the evolution of ATR-FTIR spectra as a function of temperature of the electrospun fibers to determine the changes with heating of the molecular order of the MBW derived PHBV. Moreover, in **Figure 6** the evolution with temperature of the ratio of absorbance of the bands 1230/1453 and the 1720 cm^{-1} full width at half height maximum (FWHH) for the MBW derived PHBV fibers obtained by electrospinning are represented. These two spectral features have been previously connected with the molecular order (crystallinity) in the biopolymer [45]. In particular, the strongest peak observed at 1720 cm^{-1} corresponds to the stretching vibration of the carbonyl group ν(C=O) in PHA copolyesters. Furthermore, the complex and multiple peaks that were visible in the region from 1000 cm^{-1} to 880 cm^{-1} are known to arise from to the stretching bands of the carbon–carbon single bond ν(C–C) [55]. Finally, the band centered at ∼1080 cm^{-1} was related to ester bonds in the biopolymer whereas the band at ∼1020 cm^{-1} C–O and C–O–C have been ascribed to stretching vibrations of ester groups in biopolyesters [56]. Thus, both higher 1230/1453 bands ratios and lower 1720 cm^{-1} band widths were correlated previously with higher crystallinity in the biopolymer [45].

In the ATR-FTIR spectra, it was observed that the electrospun material exhibited a continuous relative increase in the intensity of the carbonyl band, seen at 1720 cm^{-1}, among other peaks, with increasing temperature up to a maximum at around 130 ºC. The band intensity started to decrease at temperatures higher than 130 ºC. Moreover, the peak concomitantly increased its width and shifted towards higher wavenumber. From this, one can infer that the molecular order initially increased with temperature up to about 130 ºC, and after 140 ºC sharply decreased prior to melting. This annealing phenomenon was however not picked up by the 1230/1453 band ratio, which decreased monotonically with increasing temperature, being more pronounced in the vicinity of

melting, after 140 ºC. These results, but specifically the ~1720 cm^{-1} band evolution, do shed some light on the process of fibers coalescence observed by SEM, suggesting that this process takes place below the polymer melting point and is connected with a sufficiently thermally induced improvement in molecular order and the presumed mobility of the fibers during that process to reduce surface tension.

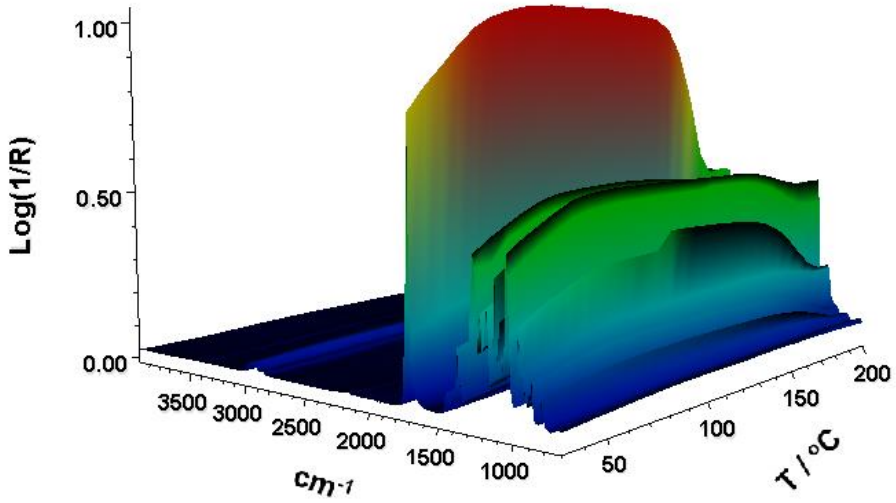

Figure 5. Fourier transform infrared (FTIR) spectra taken across temperature of the electrospun municipal biowaste (MBW) derived poly(3-hydroxybutyrate-*co*-3-hydroxyvalerate) (PHBV) fibers.

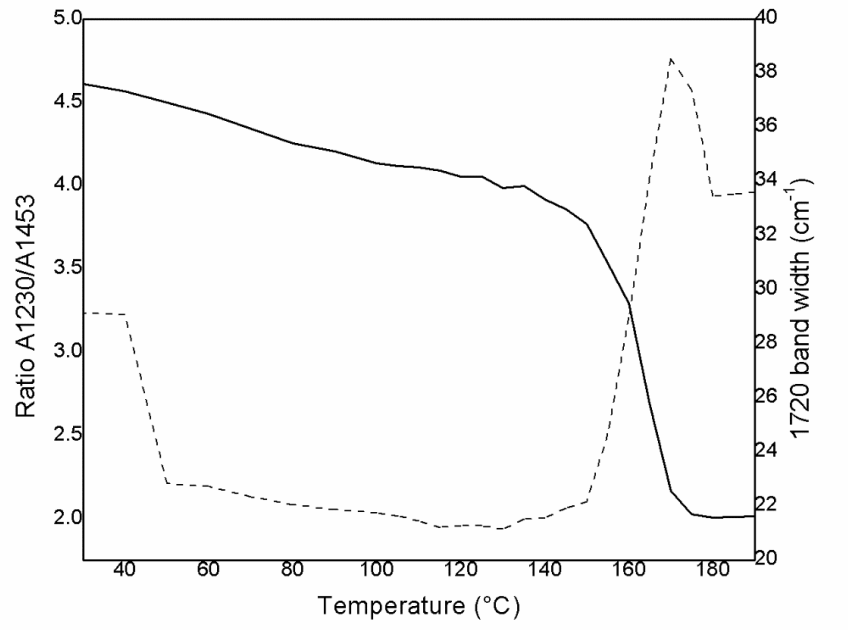

Figure 6. Evolution with temperature of the ratio of absorbance of the bands 1230/1453 (continuous line) and the 1720 cm^{-1} band full width at half height maximum (dashed line) for the electrospun municipal biowaste (MBW) derived poly(3-hydroxybutyrate-*co*-3-hydroxyvalerate) (PHBV) fibers.

The crystallinity and phase morphology of the electrospun MBW PHBV fibers was further assessed by simultaneous time-resolved SAXS and WAXD experiments as a function of temperature using synchrotron radiation. These X-ray diffraction techniques have been widely used to study crystallinity, crystalline morphology and the phase structure at the mesoscale in semicrystalline biopolymers [57]. **Figure 7** displays the simultaneous SAXS and WAXD diffractograms of the electrospun fibers in both isotherm conditions at 100 °C and 130 °C and for a thermal ramp from 0 °C to 180 °C at 10 °C/min (analogous to the DSC conditions). In the case of the isotherm at 130 °C, which intends to follow *in situ* the phase morphology alterations occurring in the sample during the annealing process, the SAXS diffractograms indicate that the peak associated with the long period [58] becomes better resolved after a few seconds at this temperature,

again supporting the FTIR observations of improved molecular order and phase structure regularity, developing during the annealing process. During the thermal ramp to melting, the SAXS peak becomes stronger with increasing temperature with maximum at ca. 130 °C, and after the peak begins to shift towards lower q values, implying an increase in long period associated with longer repeat units prior to melting. **Figure 7** also shows the WAXD diffractograms evolution over time, exhibiting the most characteristic peaks of PHB at 2θ, 8.8° and 11°, which correspond to the (020) and (110) diffractions respectively from the lattice planes of the orthorhombic unit cells of the PHB crystal [58]. The WASX diffractograms also exhibit the four minor reflections at approximately 13.5°, 16°, 17.1°, and 22°, which originate from the (021), (111), (121) and (040) lattice planes [59-60]. According to the literature, the PHB crystal lattice is characteristic for copolyesters of PHBV with HV contents below 37 mol% [61]. **Figure 8** zooms the evolution of the peak corresponding to the (110) plane for the isotherms and for the heating ramp. In the case of the isotherms, it can be clearly observed that the crystalline peak increases in relative intensity with time, especially at 130 °C, suggesting again that the crystallinity and crystalline morphology improve during the first 20 seconds of the isothermal treatment.

From the heating ramp in **Figures 7 and 8**, it was also observed that the WAXD patterns, in good agreement with the SAXS patterns behavior, undergo a relative intensity increase, suggesting a clear improvement in phase morphology and crystallinity with increasing temperature up to 130 °C, followed by a sharp decrease associated with melting beyond 150 °C, which again correlates very well with the changes observed from FTIR spectroscopy in **Figure 6**.

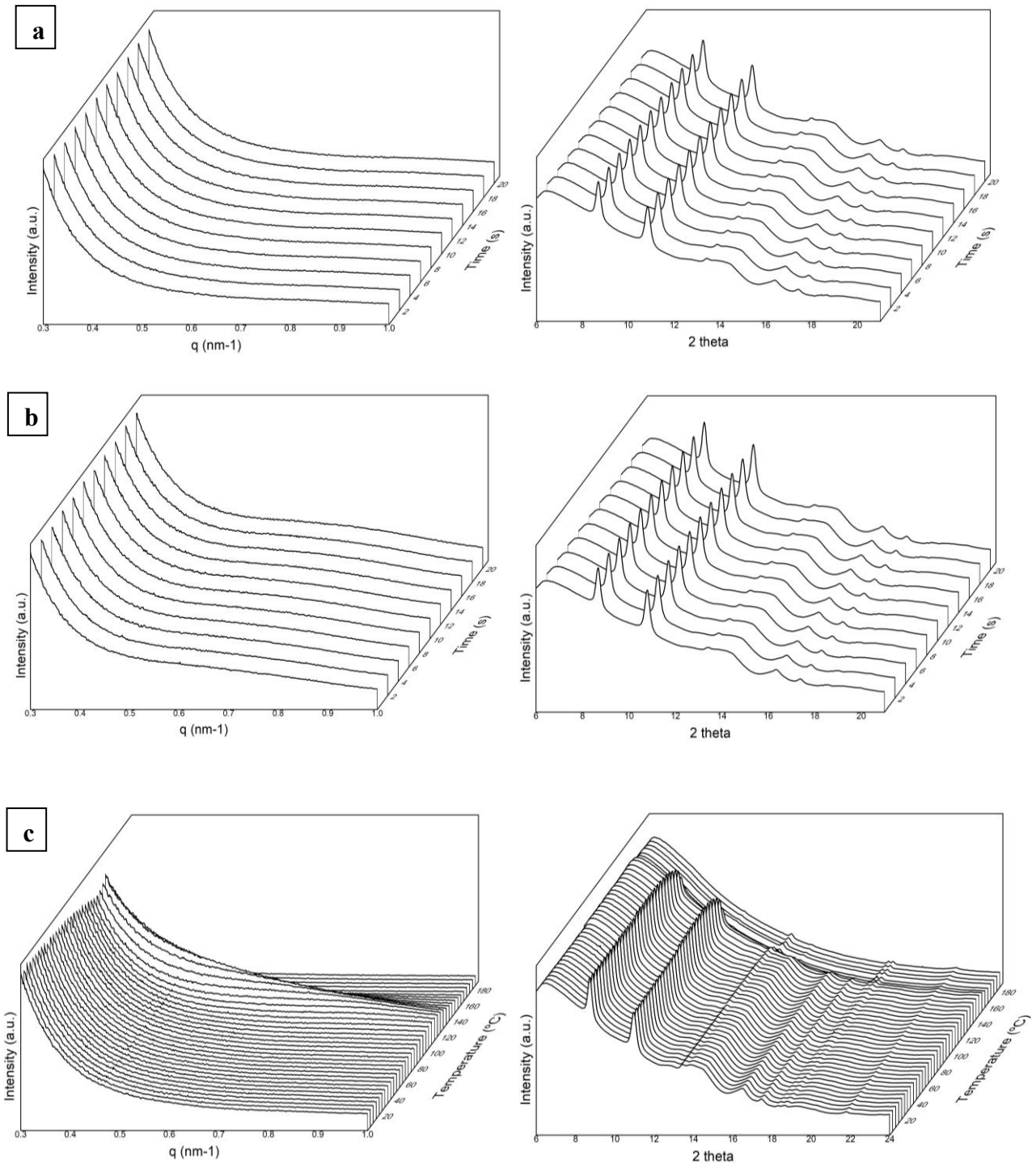
a
Intensity (a.u.)
q (nm-1)
Time (s)
2 theta
b
Intensity (a.u.)
q (nm-1)
Time (s)
2 theta
c
Intensity (a.u.)
q (nm-1)
Temperature (°C)
2 theta

Figure 7. Small angle X-Ray diffraction (SAXS) (left) and wide angle X-Ray diffraction (WAXS) (right) patterns evolution of the electrospun municipal biowaste (MBW) derived poly(3-hydroxybutyrate-*co*-3-hydroxyvalerate) (PHBV) fibers at: (a) 100 °C for 20 seconds, (b) 130 °C for 20 seconds and (c) during a thermal ramp from 0 °C up to 180 °C at 10 °C/min.

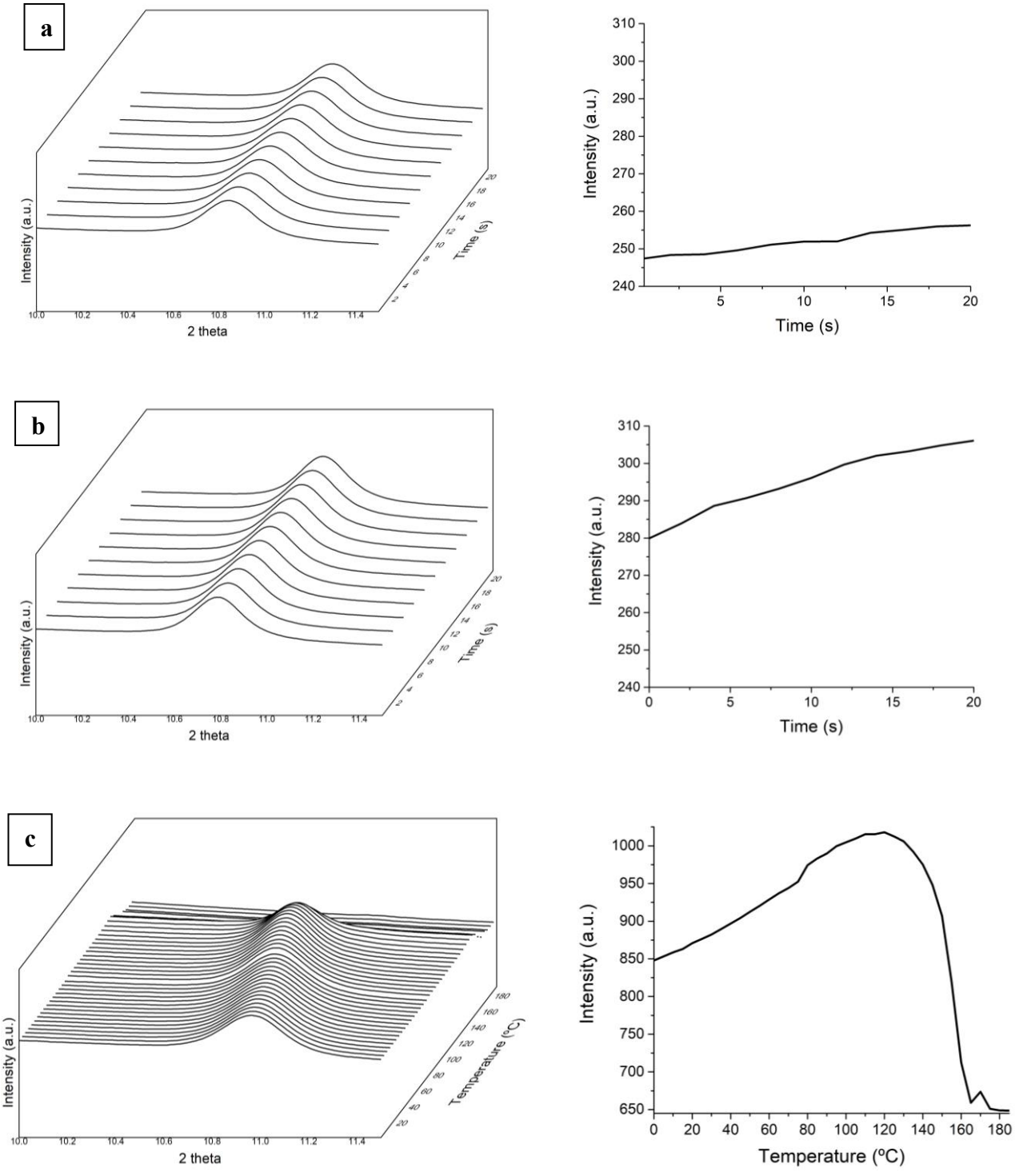

Figure 8. Wide Angle X-Ray Scattering (WAXS) patterns zoomed around the 2 theta 11º peak of the electrospun MBW derived PHBV fibers for the two isotherms (a and b) and heating ramp (c) in **Figure 7**. The right plots quantify the evolution in relative intensity of the 2 theta 11º peak seen in the left diffractograms.

3.5. Mechanical properties

Figure 9 displays the stress vs. strain curve of the MBW derived PHBV biopaper. From this curve, the values of elastic modulus (E), tensile strength at yield (σ_y), elongation at break (ε_b), and toughness (T) were obtained and are summarized in **Table 4**. From this table, it can be observed that the biopaper presented characteristic properties of a rigid and brittle material. In particular, the mean values of E and σ_y were 1583 MPa and 13.6 MPa, respectively, whereas the ε_b and T values were below 3% and 0.5 mJ/m^3, respectively. In comparison with other electrospun PHA films, the mechanical properties of the here-obtained MBW derived PHBV are close to those previously reported by Cherpinski et al. [62] who reported E and σ_y values in the range of 1000–2000 MPa and 14–28 MPa, respectively, and a ε_b value of approximately 3% for PHB and PHBV films prepared by electrospinning. Moreover, our recent studies also showed similar mechanical values for electrospun films of PHBV derived from biowaste in which the mean values of E, σ_y, and ε_b respectively were 1200 MPa, 18 MPa, and 2.5 % [17, 38]. Furthermore, when compared with PHBV films prepared by compression molding, the here-developed biopapers showed higher ductility and toughness while slightly lower mechanical strength [63-64]. These differences have been ascribed to both the inherently lower crystallinity generated by the electrospinning process and the particular film morphology being constituted by an assembly of ultrathin fibers [45]. In this regard, Alp-Erbay et al. [31] also indicated that the interactions between the coalesced fibers in the electrospun film sample (e.g. slip of fibers over one

another, point bonding, alignment, etc.) were responsible for the higher mechanical flexibility attained in the annealed electrospun materials.

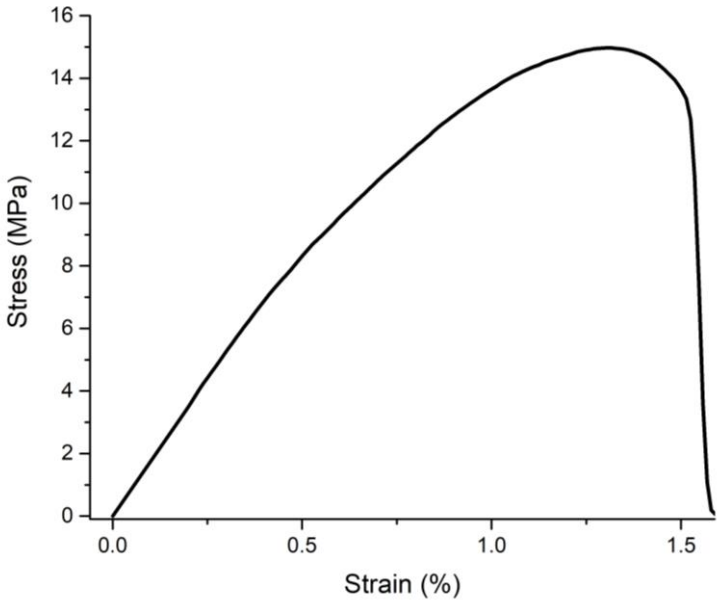

Figure 9. Typical tensile stress–strain curve of the electrospun municipal biowaste (MBW) derived poly(3-hydroxybutyrate-*co*-3-hydroxyvalerate) (PHBV) biopaper.

Table 4. Mechanical properties of the electrospun municipal biowaste (MBW) derived poly(3-hydroxybutyrate-*co*-3-hydroxyvalerate) (PHBV) biopaper in terms of: tensile modulus (E), tensile strength at yield (σ_y), elongation at break (ε_b), and toughness (T).

Biopaper	E **(MPa)**	σ_y **(MPa)**	ε_b **(%)**	**T (mJ/m^3)**
PHBV	1583 ± 249	13.6 ± 3.3	1.3 ± 0.4	0.10 ± 0.01

3.6. Barrier properties

The WVP, LP, and OP values of the electrospun MBW derived PHBV biopaper are shown in **Table 5**. It can be observed that the here-produced biopaper presented a WVP

value of 3.99 x 10^{-14} kg·m·m^{-2}·Pa^{-1}·s^{-1}, while its LP was 2.09 x 10^{-14} kg·m·m^{-2}·Pa^{-1}·s^{-1}. In comparison with others PHA films reported in the literature, the values obtained here are higher than those obtained for electrospun PHB films, that is, 5.22 x 10^{-15} kg·m·m^{-2}·Pa^{-1}·s^{-1} and 3.20 x 10^{-15} kg·m·m^{-2}·Pa^{-1}·s^{-1} for WVP and LP, respectively [45]. This barrier reduction is related to the lower crystallinity developed in the copolyester, indicating as expected that the barrier properties decrease with increasing HV content [51]. When compared with other electrospun PHBV biopapers, the here-prepared biopaper is in the same range. Thus, for PHBV with 3% HV, the values obtained were 5.3 x 10^{-14} kg·m·m^{-2}·Pa^{-1}·s^{-1} and 2.7 x 10^{-14} kg·m·m^{-2}·Pa^{-1}·s^{-1}, for WVP and LP, respectively [38]. For PHBV with higher HV content, that is, 20% HV, the values ranged between 1–3 x 10^{-14} kg·m·m^{-2}·Pa^{-1}·s^{-1}, for WVP, and 0.3–3.5 x 10^{-14} kg·m·m^{-2}·Pa^{-1}·s^{-1}, for LP [17]. In relation to PHA films prepared by other techniques, solvent-cast PHBV films showed slightly higher barrier to water and limonene vapors. In particular, the WVP was 1.27 x 10^{-14} kg·m·m^{-2}·Pa^{-1}·s^{-1} and the LP was 1.99 x 10^{-13} kg·m·m^{-2}·Pa^{-1}·s^{-1} for films made of PHBV containing 3 mol% HV [51]. Similarly, compression-molded PHB films showed a WVP of 1.7 x 10^{-15} kg·m·m^{-2}·Pa^{-1}·s^{-1} and a LP value of 8.8 x 10^{-15} kg·m·m^{-2}·Pa^{-1}·s^{-1} [65]. The slightly lower barrier performance attained for the electrospun biopaper is ascribed to the particular fiber alignment still leaving some porosity due to its fibrillar nature.

The electrospun MBW derived PHBV biopapers also present good barrier performance to oxygen. In particular, the OP value was 2.88 x 10^{-20} m^3·m·m^{-2}·Pa^{-1}·s^{-1}, which is in the range of other electrospun PHA films, such as PHBV with a 20% HV content (1.25 x 10^{-19} m^3·m·m^{-2}·Pa^{-1}·s^{-1}) [17] and PHB (1.20 x 10^{-18} m^3·m·m^{-2}·Pa^{-1}·s^{-1}) [62]. Since oxygen is more sensitive than vapours of higher molecular weight to the material free volume, defects, porosity, morphological differences, crystallinity, etc., the measured value indicates that the here-attained electrospun biopaper of PHBV derived

from MBW presents a relatively good uniformity and low porosity. In a context of packaging applications, the OP value obtained here is lower than that of polyethylene terephthalate (PET) films (1.35 x 10^{-19} $m^3 \cdot m \cdot m^{-2} \cdot Pa^{-1} \cdot s^{-1}$) but is considerably lower in comparison with that of low-density polyethylene (LDPE) films (2.15 x 10^{-17} $m^3 \cdot m \cdot m^{-2} \cdot Pa^{-1} \cdot s^{-1}$). On the other hand, the permeability to oxygen is higher than that of a high-barrier ethylene–vinyl alcohol copolymer (EVOH) (7.7 x 10^{-20} $m^3 \cdot m \cdot m^{-2} \cdot Pa^{-1} \cdot s^{-1}$) [66].

Table 5. Values of water vapor permeability (WVP), D-limonene permeability (LP), and oxygen permeability (OP) of the electrospun municipal biowaste (MBW) derived poly(3-hydroxybutyrate-*co*-3-hydroxyvalerate) (PHBV) biopaper.

Biopaper	**WVP x 10^{14} ($kg \cdot m \cdot m^{-2} \cdot Pa^{-1} \cdot s^{-1}$)**	**LP x 10^{14} ($kg \cdot m \cdot m^{-2} \cdot Pa^{-1} \cdot s^{-1}$)**	**OP x 10^{20} ($m^3 \cdot m \cdot m^{-2} \cdot Pa^{-1} \cdot s^{-1}$)**
PHBV	3.99 ± 1.32	2.09 ± 0.30	2.88 ± 0.36

4. Conclusions

In the present study, a PHBV material derived from municipal biowaste was developed, purified, run by electrospinning and post-processed by a mild thermal treatment at 130 ºC for 5 s, to obtain a fiber based continuous film so-called biopaper. The resultant film exhibited higher transparency and a less grayish color than a commercial PHBV. The thermal properties exhibited a multiple melting endotherm with maximum of melting at ca. 155 ºC. The material remained stable up to ~205 ºC, and the maximum of degradation occurred at approximately 240 ºC. Interestingly, molecular order, crystallinity and phase morphology at the mesoscale was assessed by ATR-FTIR spectroscopy and time-resolved simultaneous WAXS and SAXS experiments using

synchrotron radiation as a function of temperature, and were found to correlate very well with each other. The results indicated that by heating the electrospun fibers up until 130 ºC, the phase morphology and crystallinity are improved, beyond this temperature the crystallinity begins to deteriorate until complete melting occurs. This improvement in phase morphology upon heating, resulting from thermally activated molecular chain rearrangements allows the fibers to coalesce to reduce surface tension, and hence to reduce structural porosity. In terms of mechanical properties, the biopaper was found to exhibited a good balance between rigidity and elongation at break. Thus, the films showed higher ductility and toughness than similar PHBV films prepared by melt compounding routes. These differences were ascribed to the particular morphology of the electrospun biopaper, having ill-defined crystallinity and being composed of aligned side by side fibers. Finally, in terms of barrier properties, the biopaper showed similar values than other electrospun PHA films being slightly more permeable than their compression-molded counterpart films. In any case, the film showed high barrier to water vapor and oxygen and hence great interest in food packaging applications.

From the evidence presented, it can be concluded that the use of MBW is of significant interest to develop more environmentally compatible and economically sustainable packaging materials in full alignment with Circular Bioeconomy strategies, since the production of PHAs by these mixed microbial cultures are known to reduce the costs of the fermentation and downstream processes. Furthermore, the combination of electrospinning and a mild annealing postprocessing well below the polymer melting point, is able to yield unique PHA biopapers with balanced properties.

Acknowledgements

This research work was funded by the Spanish Ministry of Science and Innovation (MICI) through the project RTI2018-097249-B-C21, the EU H2020 YPACK project (reference number 773872) and EU H2020 USABLE project (reference number 836884). B. Melendez and S. Torres-Giner would also like to thank MICI for her FPI fellowship (BES-2016-077972) and his Juan de la Cierva–Incorporación contract (IJCI-2016-29675). The ALBA Synchrotron, Spain is also acknowledged for the funding received through the project proposal 2018022619. The authors would also like to thank the "Unidad Asociada IATA-UJI in Plastics Technology".

References

1. Koller, M., Poly(hydroxyalkanoates) for food packaging: Application and attempts towards implementation. *Applied Food Biotechnology* **2014,** *1* (1), 3-15.

2. Rehm, B. H. A., Polyester synthases: natural catalysts for plastics. *Biochem J* **2003,** *376* (Pt 1), 15-33.

3. Saharan, B.; Grewal, A.; Kumar, P., Biotechnological Production of Polyhydroxyalkanoates: A Review on Trends and Latest Developments. *Chinese Journal of Biology* **2014,** *2014*, 1-18.

4. Kourmentza, C.; Kornaros, M., Biotransformation of volatile fatty acids to polyhydroxyalkanoates by employing mixed microbial consortia: The effect of pH and carbon source. *Bioresource Technology* **2016,** *222*, 388-398.

5. Torres-Giner, S.; Montanes, N.; Fombuena, V.; Boronat, T.; Sanchez-Nacher, L., Preparation and characterization of compression-molded green composite sheets

made of poly(3-hydroxybutyrate) reinforced with long pita fibers. *Advances in Polymer Technology* **2018,** *37* (5), 1305-1315.

6. Sängerlaub, S.; Brüggemann, M.; Rodler, N.; Jost, V.; Bauer, K. D., Extrusion coating of paper with poly(3-hydroxybutyrate-co-3-hydroxyvalerate) (PHBV)-Packaging related functional properties. *Coatings* **2019,** *9* (7).

7. Acevedo, F.; Villegas, P.; Urtuvia, V.; Hermosilla, J.; Navia, R.; Seeger, M., Bacterial polyhydroxybutyrate for electrospun fiber production. *International Journal of Biological Macromolecules* **2018,** *106*, 692–697.

8. Fabra, M. J.; Lopez-Rubio, A.; Lagaron, J. M., Nanostructured interlayers of zein to improve the barrier properties of high barrier polyhydroxyalkanoates and other polyesters. *Journal of Food Engineering* **2014,** *127*, 1-9.

9. Laycock, B.; Halley, P.; Pratt, S.; Werker, A.; Lant, P., The chemomechanical properties of microbial polyhydroxyalkanoates. *Progress in Polymer Science* **2013,** *38* (3), 536-583.

10. Choi, J.-i.; Lee, S. Y., Process analysis and economic evaluation for Poly(3-hydroxybutyrate) production by fermentation. *Bioprocess Engineering* **1997,** *17* (6), 335-342.

11. Reis, M.; Albuquerque, M.; Villano, M.; Majone, M., 6.51 - Mixed Culture Processes for Polyhydroxyalkanoate Production from Agro-Industrial Surplus/Wastes as Feedstocks. In *Comprehensive Biotechnology (Second Edition)*, Moo-Young, M., Ed. Academic Press: Burlington, 2011; pp 669-683.

12. Fernández-Dacosta, C.; Posada, J. A.; Kleerebezem, R.; Cuellar, M. C.; Ramirez, A., Microbial community-based polyhydroxyalkanoates (PHAs) production

from wastewater: Techno-economic analysis and ex-ante environmental assessment. *Bioresource Technology* **2015,** *185*, 368-377.

13. Gurieff, N.; Lant, P., Comparative life cycle assessment and financial analysis of mixed culture polyhydroxyalkanoate production. *Bioresource Technology* **2007,** *98* (17), 3393-3403.

14. Albuquerque, M. G. E.; Torres, C. A. V.; Reis, M. A. M., Polyhydroxyalkanoate (PHA) production by a mixed microbial culture using sugar molasses: Effect of the influent substrate concentration on culture selection. *Water Research* **2010,** *44* (11), 3419-3433.

15. Dionisi, D.; Carucci, G.; Papini, M. P.; Riccardi, C.; Majone, M.; Carrasco, F., Olive oil mill effluents as a feedstock for production of biodegradable polymers. *Water Research* **2005,** *39* (10), 2076-2084.

16. Hassan, M. A.; Shirai, Y.; Kusubayashi, N.; Karim, M. I. A.; Nakanishi, K.; Hashimoto, K., The production of polyhydroxyalkanoate from anaerobically treated palm oil mill effluent by Rhodobacter sphaeroides. *Journal of Fermentation and Bioengineering* **1997,** *83* (5), 485-488.

17. Melendez-Rodriguez, B.; Castro-Mayorga, J. L.; Reis, M. A. M.; Sammon, C.; Cabedo, L.; Torres-Giner, S.; Lagaron, J. M., Preparation and Characterization of Electrospun Food Biopackaging Films of Poly(3-hydroxybutyrate-co-3-hydroxyvalerate) Derived From Fruit Pulp Biowaste. *Frontiers in Sustainable Food Systems* **2018,** *2*, 38.

18. Melendez-Rodriguez, B.; Torres-Giner, S.; Figueroa-Lopez, K. J.; Castro-Mayorga, J. L.; Lagaron, J. M.; Cabedo, L. In *On the use of high-throughput*

electrospinning to produce optimized packaging films from polyhydroxyalkanoates, Annual Technical Conference - ANTEC, Conference Proceedings, 2018.

19. Colombo, B.; Pepè Sciarria, T.; Reis, M.; Scaglia, B.; Adani, F., Polyhydroxyalkanoates (PHAs) production from fermented cheese whey by using a mixed microbial culture. *Bioresource Technology* **2016,** *218*, 692-699.

20. Morgan-Sagastume, F.; Hjort, M.; Cirne, D.; Gérardin, F.; Lacroix, S.; Gaval, G.; Karabegovic, L.; Alexandersson, T.; Johansson, P.; Karlsson, A.; Bengtsson, S.; Arcos-Hernández, M. V.; Magnusson, P.; Werker, A., Integrated production of polyhydroxyalkanoates (PHAs) with municipal wastewater and sludge treatment at pilot scale. *Bioresource Technology* **2015,** *181*, 78-89.

21. Mata-Alvarez, J.; Dosta, J.; Romero-Güiza, M. S.; Fonoll, X.; Peces, M.; Astals, S., A critical review on anaerobic co-digestion achievements between 2010 and 2013. *Renewable and Sustainable Energy Reviews* **2014,** *36*, 412-427.

22. Korkakaki, E.; Mulders, M.; Veeken, A.; Rozendal, R.; van Loosdrecht, M. C. M.; Kleerebezem, R., PHA production from the organic fraction of municipal solid waste (OFMSW): Overcoming the inhibitory matrix. *Water Research* **2016,** *96*, 74-83.

23. Zhang, M.; Wu, H.; Chen, H., Coupling of polyhydroxyalkanoate production with volatile fatty acid from food wastes and excess sludge. *Process Safety and Environmental Protection* **2014,** *92* (2), 171-178.

24. Coats, E. R.; Loge, F. J.; Wolcott, M. P.; Englund, K.; McDonald, A. G., Synthesis of Polyhydroxyalkanoates in Municipal Wastewater Treatment. *Water Environment Research* **2007,** *79* (12), 2396-2403.

25. Doshi, J.; Reneker, D. H., Electrospinning process and applications of electrospun fibers. *Journal of Electrostatics* **1995,** *35* (2), 151-160.

26. Torres-Giner, S.; Pérez-Masiá, R.; Lagaron, J. M., A review on electrospun polymer nanostructures as advanced bioactive platforms. *Polymer Engineering and Science* **2016,** *56* (5), 500-527.

27. Cherpinski, A.; Torres-Giner, S.; Cabedo, L.; Méndez, J. A.; Lagaron, J. M., Multilayer structures based on annealed electrospun biopolymer coatings of interest in water and aroma barrier fiber-based food packaging applications. *Journal of Applied Polymer Science* **2018,** *135* (24).

28. Cherpinski, A.; Torres-Giner, S.; Vartiainen, J.; Peresin, M. S.; Lahtinen, P.; Lagaron, J. M., Improving the water resistance of nanocellulose-based films with polyhydroxyalkanoates processed by the electrospinning coating technique. *Cellulose* **2018,** *25* (2), 1291-1307.

29. Spagnol, C.; Fragal, E. H.; Pereira, A. G. B.; Nakamura, C. V.; Muniz, E. C.; Follmann, H. D. M.; Silva, R.; Rubira, A. F., Cellulose nanowhiskers decorated with silver nanoparticles as an additive to antibacterial polymers membranes fabricated by electrospinning. *Journal of Colloid and Interface Science* **2018,** *531*, 705-715.

30. Hu, M.; Li, C.; Li, X.; Zhou, M.; Sun, J.; Sheng, F.; Shi, S.; Lu, L., Zinc oxide/silver bimetallic nanoencapsulated in PVP/PCL nanofibres for improved antibacterial activity. *Artificial Cells, Nanomedicine, and Biotechnology* **2018,** *46* (6), 1248-1257.

31. Alp-Erbay, E.; Figueroa-Lopez, K. J.; Lagaron, J. M.; Çağlak, E.; Torres-Giner, S., The impact of electrospun films of poly(ε-caprolactone) filled with nanostructured

zeolite and silica microparticles on in vitro histamine formation by Staphylococcus aureus and Salmonella Paratyphi A. *Food Packaging and Shelf Life* **2019,** *22*.

32. Quiles-Carrillo, L.; Montanes, N.; Lagaron, J. M.; Balart, R.; Torres-Giner, S., Bioactive multilayer polylactide films with controlled release capacity of gallic acid accomplished by incorporating electrospun nanostructured coatings and interlayers. *Applied Sciences (Switzerland)* **2019,** *9* (3).

33. Cherpinski, A.; Gozutok, M.; Sasmazel, H. T.; Torres-Giner, S.; Lagaron, J. M., Electrospun oxygen scavenging films of poly(3-hydroxybutyrate) containing palladium nanoparticles for active packaging applications. *Nanomaterials* **2018,** *8* (7).

34. Lasprilla-Botero, J.; Torres-Giner, S.; Pardo-Figuerez, M.; álvarez-Láinez, M.; Lagaron, J. M., Superhydrophobic bilayer coating based on annealed electrospun ultrathin poly(ε-caprolactone) fibers and electrosprayed nanostructured silica microparticles for easy emptying packaging applications. *Coatings* **2018,** *8* (5).

35. Torres-Giner, S.; Echegoyen, Y.; Teruel-Juanes, R.; Badia, J. D.; Ribes-Greus, A.; Lagaron, J. M., Electrospun Poly(ethylene-co-vinyl alcohol)/Graphene Nanoplatelets Composites of Interest in Intelligent Food Packaging Applications. *Nanomaterials* **2018,** *8* (10).

36. Valentino, F.; Moretto, G.; Lorini, L.; Bolzonella, D.; Pavan, P.; Majone, M., Pilot-Scale Polyhydroxyalkanoate Production from Combined Treatment of Organic Fraction of Municipal Solid Waste and Sewage Sludge. *Industrial & Engineering Chemistry Research* **2019,** *58* (27), 12149-12158.

37. Fiorese, M. L.; Freitas, F.; Pais, J.; Ramos, A. M.; De Aragão, G. M. F.; Reis, M. A. M., Recovery of polyhydroxybutyrate (PHB) from Cupriavidus necator biomass

by solvent extraction with 1,2-propylene carbonate. *Engineering in Life Sciences* **2009,** *9* (6), 454-461.

38. Melendez-Rodriguez, B.; Figueroa-Lopez, J. K.; Bernardos, A.; Martínez-Máñez, R.; Cabedo, L.; Torres-Giner, S.; M. Lagaron, J., Electrospun Antimicrobial Films of Poly(3-hydroxybutyrate-co-3-hydroxyvalerate) Containing Eugenol Essential Oil Encapsulated in Mesoporous Silica Nanoparticles. *Nanomaterials* **2019,** *9* (2).

39. Shiku, Y.; Yuca Hamaguchi, P.; Benjakul, S.; Visessanguan, W.; Tanaka, M., Effect of surimi quality on properties of edible films based on Alaska pollack. *Food Chemistry* **2004,** *86* (4), 493-499.

40. Kanatt, S. R.; Rao, M. S.; Chawla, S. P.; Sharma, A., Active chitosan–polyvinyl alcohol films with natural extracts. *Food Hydrocolloids* **2012,** *29* (2), 290-297.

41. Arfat, Y. A.; Ahmed, J.; Hiremath, N.; Auras, R.; Joseph, A., Thermo-mechanical, rheological, structural and antimicrobial properties of bionanocomposite films based on fish skin gelatin and silver-copper nanoparticles. *Food Hydrocolloids* **2017,** *62*, 191-202.

42. Mokrzycki, W.; Tatol, M., Color difference Delta E - A survey. *Machine Graphics and Vision* **2011,** *20*, 383-411.

43. Kunasundari, B.; Sudesh, K., Isolation and recovery of microbial polyhydroxyalkanoates. *Express Polymer Letters* **2011,** *5* (7), 620-634.

44. Torres-Giner, S.; Wilkanowicz, S.; Melendez-Rodriguez, B.; Lagaron, J. M., Nanoencapsulation of Aloe vera in Synthetic and Naturally Occurring Polymers by Electrohydrodynamic Processing of Interest in Food Technology and Bioactive Packaging. *Journal of Agricultural and Food Chemistry* **2017,** *65* (22), 4439-4448.

45. Cherpinski, A.; Torres-Giner, S.; Cabedo, L.; Lagaron, J. M., Post-processing optimization of electrospun submicron poly(3-hydroxybutyrate) fibers to obtain continuous films of interest in food packaging applications. *Food Additives and Contaminants - Part A Chemistry, Analysis, Control, Exposure and Risk Assessment* **2017,** *34* (10), 1817-1830.

46. Figueroa-Lopez, K. J.; Torres-Giner, S.; Enescu, D.; Cabedo, L.; Cerqueira, M. A.; Pastrana, L. M.; Lagaron, J. M., Electrospun Active Biopapers of Food Waste Derived Poly(3-hydroxybutyrate-co-3-hydroxyvalerate) with Short-Term and Long-Term Antimicrobial Performance. *Nanomaterials* **2020,** *10* (3), 506.

47. Figueroa-Lopez, K. J.; Vicente, A. A.; Reis, M. A. M.; Torres-Giner, S.; Lagaron, J. M., Antimicrobial and Antioxidant Performance of Various Essential Oils and Natural Extracts and Their Incorporation into Biowaste Derived Poly(3-hydroxybutyrate-co-3-hydroxyvalerate) Layers Made from Electrospun Ultrathin Fibers. *Nanomaterials* **2019,** *9* (2), 144.

48. Melendez-Rodriguez, B.; Torres-Giner, S.; Aldureid, A.; Cabedo, L.; Lagaron, J. M., Reactive Melt Mixing of Poly(3-Hydroxybutyrate)/Rice Husk Flour Composites with Purified Biosustainably Produced Poly(3-Hydroxybutyrate-co-3-Hydroxyvalerate). *Materials* **2019,** *12* (13), 2152.

49. Jung, H.-R.; Choi, T.-R.; Han, Y. H.; Park, Y.-L.; Park, J. Y.; Song, H.-S.; Yang, S.-Y.; Bhatia, S. K.; Gurav, R.; Park, H.; Namgung, S.; Choi, K.-Y.; Yang, Y.-H., Production of blue-colored polyhydroxybutyrate (PHB) by one-pot production and coextraction of indigo and PHB from recombinant Escherichia coli. *Dyes and Pigments* **2020,** *173*, 107889.

50. Zhang, K.; Misra, M.; Mohanty, A. K., Toughened sustainable green composites from poly(3-hydroxybutyrate-co-3-hydroxyvalerate) based ternary blends and miscanthus biofiber. *ACS Sustainable Chemistry and Engineering* **2014,** *2* (10), 2345-2354.

51. Sanchez-Garcia, M. D.; Gimenez, E.; Lagaron, J. M., Morphology and barrier properties of solvent cast composites of thermoplastic biopolymers and purified cellulose fibers. *Carbohydrate Polymers* **2008,** *71* (2), 235-244.

52. Castro Mayorga, J. L.; Fabra Rovira, M. J.; Cabedo Mas, L.; Sánchez Moragas, G.; Lagarón Cabello, J. M., Antimicrobial nanocomposites and electrospun coatings based on poly(3-hydroxybutyrate-co-3-hydroxyvalerate) and copper oxide nanoparticles for active packaging and coating applications. *Journal of Applied Polymer Science* **2018,** *135* (2).

53. Castro-Mayorga, J. L.; Fabra, M. J.; Lagaron, J. M., Stabilized nanosilver based antimicrobial poly(3-hydroxybutyrate-co-3-hydroxyvalerate) nanocomposites of interest in active food packaging. *Innovative Food Science and Emerging Technologies* **2016,** *33*, 524-533.

54. Castro-Mayorga, J. L.; Fabra, M. J.; Pourrahimi, A. M.; Olsson, R. T.; Lagaron, J. M., The impact of zinc oxide particle morphology as an antimicrobial and when incorporated in poly(3-hydroxybutyrate-co-3-hydroxyvalerate) films for food packaging and food contact surfaces applications. *Food and Bioproducts Processing* **2017,** *101*, 32-44.

55. Torres-Giner, S.; Montanes, N.; Boronat, T.; Quiles-Carrillo, L.; Balart, R., Melt grafting of sepiolite nanoclay onto poly(3-hydroxybutyrate-co-4-hydroxybutyrate) by

reactive extrusion with multi-functional epoxy-based styrene-acrylic oligomer. *European Polymer Journal* **2016,** *84*, 693-707.

56. Torres-Giner, S.; Gimeno-Alcañiz, J. V.; Ocio, M. J.; Lagaron, J. M., Optimization of electrospun polylactide-based ultrathin fibers for osteoconductive bone scaffolds. *Journal of Applied Polymer Science* **2011,** *122* (2), 914-925.

57. Riekel, C.; García Gutiérrez, M. C.; Gourrier, A.; Roth, S., Recent synchrotron radiation microdiffraction experiments on polymer and biopolymer fibers. *Analytical and Bioanalytical Chemistry* **2003,** *376* (5), 594-601.

58. Sato, H.; Suttiwijitpukdee, N.; Hashimoto, T.; Ozaki, Y., Simultaneous Synchrotron SAXS/WAXD Study of Composition Fluctuations, Cold-Crystallization, and Melting in Biodegradable Polymer Blends of Cellulose Acetate Butyrate and Poly(3-hydroxybutyrate). *Macromolecules* **2012,** *45* (6), 2783-2795.

59. Vahabi, H.; Michely, L.; Moradkhani, G.; Akbari, V.; Cochez, M.; Vagner, C.; Renard, E.; Saeb, M. R.; Langlois, V., Thermal Stability and Flammability Behavior of Poly(3-hydroxybutyrate) (PHB) Based Composites. *Materials (Basel)* **2019,** *12* (14), 2239.

60. Panaitescu, D. M.; Nicolae, C. A.; Frone, A. N.; Chiulan, I.; Stanescu, P. O.; Draghici, C.; Iorga, M.; Mihailescu, M., Plasticized poly(3-hydroxybutyrate) with improved melt processing and balanced properties. *Journal of Applied Polymer Science* **2017,** *134* (19).

61. Škrbić, Z.; Divjaković, V., Temperature influence on changes of parameters of the unit cell of biopolymer PHB. *Polymer* **1996,** *37* (3), 505-507.

62. Cherpinski, A.; Torres-Giner, S.; Vartiainen, J.; Peresin, M. S.; Lahtinen, P.; Lagaron, J. M., Improving the water resistance of nanocellulose-based films with polyhydroxyalkanoates processed by the electrospinning coating technique. *Cellulose* **2018**, 1-17.

63. Torres-Giner, S.; Hilliou, L.; Melendez-Rodriguez, B.; Figueroa-Lopez, K. J.; Madalena, D.; Cabedo, L.; Covas, J. A.; Vicente, A. A.; Lagaron, J. M., Melt processability, characterization, and antibacterial activity of compression-molded green composite sheets made of poly(3-hydroxybutyrate-co-3-hydroxyvalerate) reinforced with coconut fibers impregnated with oregano essential oil. *Food Packaging and Shelf Life* **2018,** *17*, 39-49.

64. Shibata, M.; Oyamada, S.; Kobayashi, S.-i.; Yaginuma, D., Mechanical properties and biodegradability of green composites based on biodegradable polyesters and lyocell fabric. *Journal of Applied Polymer Science* **2004,** *92* (6), 3857-3863.

65. Sanchez-Garcia, M. D.; Gimenez, E.; Lagaron, J. M., Novel PET nanocomposites of interest in food packaging applications and comparative barrier performance with biopolyester nanocomposites. *Journal of Plastic Film and Sheeting* **2007,** *23* (2), 133-148.

66. Lagarón, J. M., Multifunctional and nanoreinforced polymers for food packaging. In *Multifunctional and Nanoreinforced Polymers for Food Packaging*, 2011; pp 1-28.